Mon. Not. R. Astron. Soc. **000**, 000–000 (2008)

Close Approach during Hard Binary–Binary Scattering

D. Bacon[1], S. Sigurdsson[2,3] and M. B. Davies[2]
[1] *Jesus College, Cambridge CB5 8BL*
[2] *Institute of Astronomy, Madingley Road, Cambridge CB3 OHA*
[3] *Author to whom inquiries should be directed.*

Received ** *** 1995; in original form 1995 *** **

ABSTRACT
It is now clear that there is a substantial population of primordial binaries in galactic globular clusters and that binary interactions are a major influence on globular cluster evolution. Collisional interactions involving stars in binaries may provide a significant channel for the formation of various stellar exotica, such as blue stragglers, X–ray binaries and millisecond pulsars. We report on an extensive series of numerical experiments of binary–binary scattering, analysing the cross–section for close approach during interactions for a range of hard binary parameters of interest in globular cluster cores. We consider the implied rate for tidal interactions for different globular clusters and compare our results with previous, complementary estimates of stellar collision rates in globular clusters. We find that the collision rate for binary–binary encounters dominates in low density clusters if the binary fraction in the cluster is larger than 0.2 for wide main–sequence binaries. In dense clusters binary–single interactions dominate the collision rate and the core binary fraction must be $\lesssim 0.1$ per decade in semi–major axis or too many collisions take place compared to observations. The rates are consistent if binaries with semi–major axes $\sim 100AU$ are overabundant in low density clusters or if breakup and ejection substantially lowers the binary fraction in denser clusters. Given reasonable assumptions about fractions of binaries in the cores of low density clusters such as NGC 5053, we cannot account for all the observed blue stragglers by stellar collisions during binary encounters, suggesting a substantial fraction may be due to coalescence of tight primordial binaries.

Key words: stellar: binaries, dynamics – globular clusters: dynamics

1 INTRODUCTION

As the evidence for the presence of primordial binaries in globular clusters increases, it has become clear that the contribution of binary–single star and binary–binary scattering to stellar collisions and other stellar binary processes must be significant, at least in some clusters (see reviews by Hut *et al.* 1992; Livio 1995; also, Sigurdsson & Phinney 1995, Davies 1995, Davies & Benz 1995, Leonard 1989, Goodman & Hut 1989). Of particular importance are tidal encounters, or stellar collisions, that occur during resonances that develop during hard binary–single and binary–binary scatterings. These may contribute significantly to the formation of blue stragglers (Leonard 1989, Leonard & Fahlman 1991, Leonard & Linnell 1992), X–ray binaries, MSPs, CVs runaway stars and other exotica (Sigurdsson & Phinney 1995, Davies 1995).

Binary–binary scattering may be particularly important in low-density clusters where there may be a large number of primordial binaries and products of binary interactions such as blue stragglers (Hills 1975, Nemec & Harris 1987, Nemec & Cohen 1989, Leonard 1989, Mateo *et al.* 1990, Bolte 1991, Hills 1992, Leonard & Linnell 1992, Bolte *et al.* 1993, Yan & Mateo 1994). Mass segregation effects in globular clusters will increase the binary fraction in the core compared to the rest of the cluster. Thus, even if the binary fraction in the whole cluster is low (say $\sim 5\%$) the fraction in the core may be much higher (see, for example, Leonard 1989, Hut *et al.* 1992, McMillan & Hut 1994, but note also Sigurdsson & Phinney 1995).

Here we report the results of 100,000 numerical experiments of hard binary–binary scatterings, for a range of binary parameters appropriate to globular cluster interactions. Other studies of binary–binary encounters have been carried out (Mikkola 1983, 1984a,b, Hoffer 1983, Leonard 1989, Leonard & Fahlman 1991, McMillan *et al.* 1990, 1991, Hut *et al.* 1992, Hut 1995, Rasio *et al.* 1995). Mikkola considered a range of hard and soft binary scatterings looking at the final state and energy transfer, while Hoffer included mostly soft binary encounters. Leonard's work overlaps with ours, but does not present a systematic survey of cumulative cross–sections as reported here, and our work should be consid-

ered complementary to his. McMillan, Hut and Rasio have so far mostly reported studies of particular sets of encounters or encounters in particular models of clusters rather than surveys of cross–sections. We present a set of cumulative cross–sections for close approach during hard encounters for a range of mass ratios and semi–major axis ratios. We compute the relative event rate for the various possible outcomes of the encounters. We also present sample cross–sections for the change in semi–major axis during flybys and compare them to the one seen in encounters between binaries and single stars. We leave a detailed discussion of the subsequent evolution of the systems produced in encounters, such as triple-star systems, to a later paper.

The cross–sections for close approaches calculated here complement previous hydrodynamical calculations of the outcome of stellar collisions and strong tidal interactions in the context of hard binary encounters (Davies *et al.* 1994, Davies & Benz 1995, Goodman & Hernquist 1991, Sigurdsson & Hernquist 1992).

2 METHOD

The initial conditions for the scatterings were set following the method of Hut & Bahcall (1983, see also Sigurdsson & Phinney 1993). With two binaries, we have additional parameters from the relative phase of the second binary, the orientation of the plane of the second binary and the second binary mass ratio, semi–major axis and eccentricity. We drew the binary parameters by Monte Carlo selection uniformly over the phase variables. The relative velocity at infinity of the centres–of–mass of the two binaries, v_∞ was chosen uniformly on the interval allowed. We refer to a set of encounters performed at fixed a_i, M_i and range of v_∞ as a "run". A discrete set of values for the semi–major axis, a_1, a_2 and masses, M_1, M_2, M_3, M_4 was used for each run. The binary eccentricities, $e_{1,2}$ were zero for all encounters reported here; previous calculations indicate the cross–sections of interest are not sensitive to the binaries' eccentricities. We discuss the limitations of this assumption later in this paper. For the runs discussed here the binary parameters used are shown in Table 1.

The critical velocity, v_c, is the velocity for which the total energy of the system in the centre–of–mass frame is zero, is given by

$$v_c^2 = \frac{G}{\mu}\left(\frac{M_1 M_2}{a_1} + \frac{M_3 M_4}{a_2}\right) \tag{1}$$

where $\mu = (M_1+M_2)(M_3+M_4)/M_T$, $M_T = M_1+M_2+M_3+M_4$, is the binaries reduced mass, and a_1, a_2 are the semi–major axes of the binaries containing masses $M_{1,2}, M_{3,4}$ respectively. Note that for these simulations $M_1 = M_3$ and $M_2 = M_4$. As a convention we order $a_1 \geq a_2$, $M_{1,3} \geq M_{2,4}$, and choose $G = 1$. The sampling in velocity was uniform in v_∞/v_c over the range indicated for each set of runs shown.

We refer to encounters where $v_\infty/v_c \leq 1$ as "hard", following the nomenclature established for binary–single scatterings. Hard encounters are dominated by gravitational focusing. Treating the binaries as point masses at each binary centre–of–mass, for an impact parameter b, the pericentre, p is given by

Table 1. The properties of all the runs performed.

Run	Variables						
	v_∞/v_c	a_1	a_2	$M_{1,3}$	$M_{2,4}$	v_c^2	N
10d	1/8-1/4	1.0	1.0	1.0	1.0	2	4000
11d	1/4-1/2	1.0	1.0	1.0	1.0		4000
12d	1/2-1	1.0	1.0	1.0	1.0		4000
13d	1/16-1/8	1.0	1.0	1.0	1.0		4000
20d	1/8-1/4	1.0	1.0	1.0	0.5	4/3	4000
21d	1/4-1/2	1.0	1.0	1.0	0.5		4000
22d	1/2-1	1.0	1.0	1.0	0.5		4000
10r	1/8-1/4	2.0	0.5	1.0	1.0	5/2	4000
11r	1/4-1/2	2.0	0.5	1.0	1.0		4000
12r	1/2-1	2.0	0.5	1.0	1.0		4000
20r	1/8-1/4	2.0	0.5	1.0	0.5	5/3	4000
21r	1/4-1/2	2.0	0.5	1.0	0.5		4000
22r	1/2-1	2.0	0.5	1.0	0.5		4000
30r	1/8-1/4	$\sqrt{2}$	$1/\sqrt{2}$	1.0	1.0	$3/\sqrt{2}$	4000
31r	1/4-1/2	$\sqrt{2}$	$1/\sqrt{2}$	1.0	1.0		4000
32r	1/2-1	$\sqrt{2}$	$1/\sqrt{2}$	1.0	1.0		4000
40r	1/8-1/4	$\sqrt{2}$	$1/\sqrt{2}$	1.0	0.5	$2/\sqrt{2}$	4000
41r	1/4-1/2	$\sqrt{2}$	$1/\sqrt{2}$	1.0	0.5		4000
42r	1/2-1	$\sqrt{2}$	$1/\sqrt{2}$	1.0	0.5		4000
50r	1/8-1/4	4.0	0.25	1.0	1.0	17/4	4000
51r	1/4-1/2	4.0	0.25	1.0	1.0		4000
52r	1/2-1	4.0	0.25	1.0	1.0		4000
60r	1/8-1/4	4.0	0.25	1.0	0.5	17/6	4000
61r	1/4-1/2	4.0	0.25	1.0	0.5		4000
62r	1/2-1	4.0	0.25	1.0	0.5		4000

$$p = \frac{GM_T}{v_\infty^2}\left(\left(1 + b^2\left(\frac{v_\infty^2}{GM_T}\right)^2\right)^{1/2} - 1\right). \tag{2}$$

For $v_\infty/v_c \ll 1$, $p \approx b^2 v_\infty^2/2GM_T$. The impact parameter for each scattering is uniform in b^2 to some maximum impact parameter b_{max}. By extension of Hut & Bahcall's choice (1983) we set $b_{max} = Ca_1/v_\infty + Da_1$, where $C = 5, D = 0.6$ for the set of runs reported here. For $v_\infty/v_c \ll 1$,

$$p_{max} = \frac{C^2 a_1^2}{2GM_T}\left(1 + \frac{Dv_\infty}{C}\right)^2. \tag{3}$$

Note for $a_1 \gg a_2$ the maximum pericentre approach is large compared to a_2; this is necessary as the wider binary may be sensitive to perturbations from the tighter binary at several a_1, while the tighter binary will likely be only very weakly perturbed. Thus for $a_1/a_2 \gg 1$ we have to sample the scatterings to large impact parameter. For $a_1 = 4a_2$ and $a_1 = 16a_2$ we carried out a separate run with $C = 4$ to check the cross–section for very close approaches had converged and we were sampling the strong interactions adequately. The runs with $C = 5$ proved adequate and results from those are reported here to provide a homogenous sample. The results from the smaller impact parameter runs will be discussed in a later paper.

While the simulations are scale free, the choice of masses and v_∞/v_c were made bearing in mind the physically interesting range of velocities in globular clusters, $v_\infty \sim 10\mathrm{km\,s^{-1}}$

and $M_i = 0.5 - 1.5\mathrm{M}_\odot$. Of particular interest are wide ($a_i \sim 1 - 100\,AU$) binaries containing main–sequence stars near the turnoff ($M_i \approx 0.7\mathrm{M}_\odot$), neutron stars ($M_i \approx 1.4\mathrm{M}_\odot$) and white dwarfs ($M_i \sim 0.5 - 1.2\mathrm{M}_\odot$).

2.1 Integration scheme

Two integration schemes were used in the calculations: a fourth order Runge–Kutta integration scheme with adaptive step size and quality control (see Hut & Bahcall 1983, Sigurdsson & Phinney 1993), and a Bulirsch–Stoer variable step integrator with KS–chain regularisation (Aarseth 1984, Mikkola 1983, 1984a,b). The Runge–Kutta scheme is simple to implement and provided a direct comparison with previous binary–single scatterings. However, for $a_1/a_2 \gtrsim 2$ the step size necessary to prevent secular drift in the total energy of the system becomes prohibitively small, and the Bulirsch–Stoer regularised scheme is an order of magnitude faster in integration despite the higher cost per integration step. The Bulirsch–Stoer regularised scheme is more complicated to implement and we relied heavily on subroutines provided by Sverre Aarseth. Typically the Runge–Kutta integration for $a_1 = a_2$ required $\gtrsim 10^5$ steps to resolve a hard encounter, while the Bulirsch–Stoer regularised scheme typically required $\lesssim 10^4$ steps.

As the Bulirsch–Stoer scheme uses large integration steps, there is concern that it may not accurately track the true close approach pair separations. We note that the cross–sections from the set of runs carried out with the Runge–Kutta integration scheme agreed to within statistical error with the cross–sections calculated by the Bulirsch–Stoer regularised integrator for the same sets of parameters. We also varied the parameter for integration tolerance by two orders of magnitude for one set of runs, forcing a smaller integration step size, and checked that the cross–sections did not change with the integration step size. Here we report a homogenous set of runs done only with the Bulirsch–Stoer regularised scheme.

The code was run on a DEC 3000/400 alpha, and the total set of runs required about 3 weeks of cpu time. During each encounter the true pairwise separation between each pair of particles was monitored and the minimum value of each was stored. In addition we stored the position and velocity of all four particles at the moment of the single closest pair approach. This was for future analysis of the properties of the remnant system for particles deemed to have undergone a strong tidal encounter of collision. As the simulations are scale free, we chose not to pick a scale and allow tidal interactions to occur during the encounter, rather we analyse the outcome using a "sticky particle approximation" with a variable scale picked for each run after the runs are completed (Sigurdsson & Phinney 1993, Davies *et al.* 1994). The analysis using the sticky particle approximation will be discussed in a later paper (in preparation). The position and velocities saved at closest approach also permit generation of initial conditions for SPH simulations by time reversing the integration from the point of closest approach to a suitable initial separation (see Sigurdsson & Hernquist 1992).

The integration was stopped when either a maximum number of integration steps had been taken, 2,000,000 for Runge–Kutta integration, 500,000 for Bulirsch–Stoer integration; or when two of the pair separations, r_{ij}, exceeded some critical value $R_m = 1.2 \times R_{in}$ where $R_{in} = 30 \times \max\{a_1, a_2\}$ was the initial binary separation.

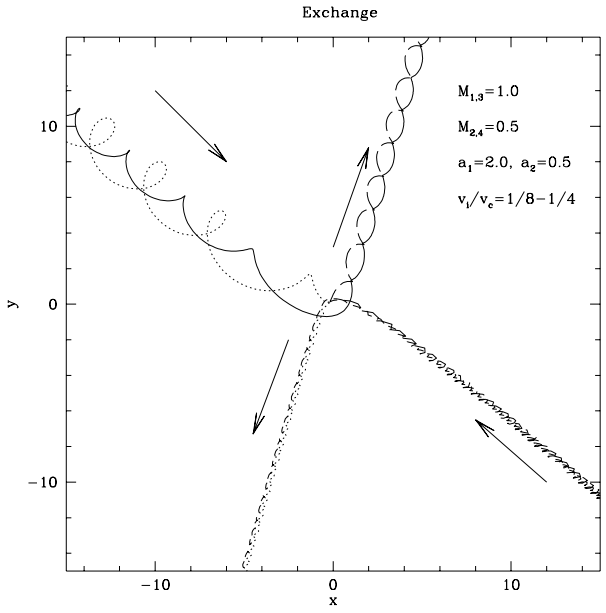

Figure 1. An example of an exchange during an encounter between unequal mass binaries with different semi–major axis.

2.2 Possible Outcomes

There are several possible outcomes of encounters between two binaries. In a flyby the two binaries may remain intact, with the components remaining unchanged, but the orbital parameters of each binary may be perturbed, possibly strongly. Alternatively an exchange encounter may occur, where components of the two binaries are exchanged, producing two new binaries. The trajectories of the four stars during such an encounter are shown in Figure 1. Another possibility is that one binary may be broken up resulting in the ejection of two single stars (as illustrated in Figure 2), or one star may be ejected leaving the three remaining stars in a triple. The formation of a triple-star system is shown in Figure 3. Since we only consider hard encounters where the total centre–of–mass energy is negative, it is not possible for both binaries to be broken up by an encounter.

Table 2 shows the number of different outcomes for each of the runs discussed here. As expected, the effectively larger maximum pericentres for encounters with $a_1/a_2 \gg 1$ leads to proportionally more flybys in those runs.

The outcome of each encounter was analysed after the run was complete to determine the final state of the binaries. We do the final analysis of outcome after the runs are terminated rather than "on the fly". It is necessary to do the analysis after the runs, because the termination conditions are not exact and may lead to excessively long integrations for individual encounters, to carry out the simulations in a reasonably short time some fraction of unresolved encounters must be accepted. The pair of particles with the highest specific binding energy was determined; this pair is assumed

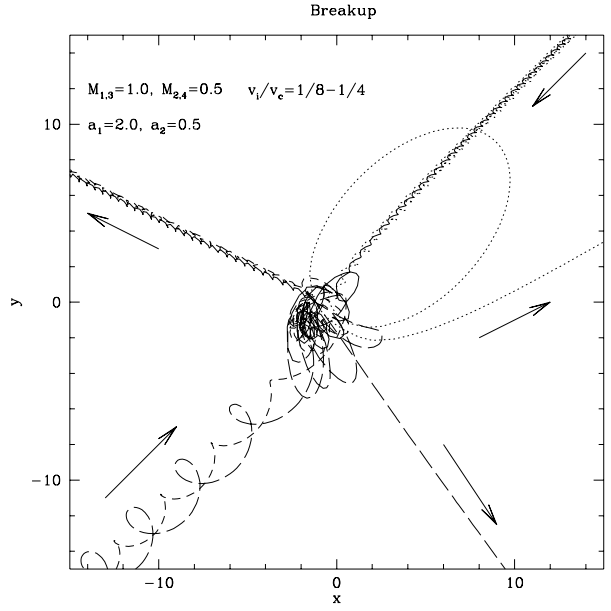

Figure 2. An example of a breakup of a binary during a resonant encounter between two binaries of unequal mass and semi–major axis.

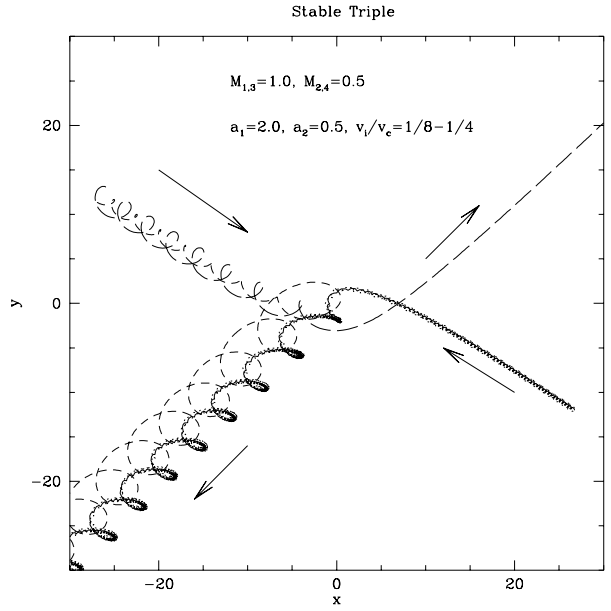

Figure 3. A figure showing the ejection of a single star and the formation of a triple-star system. As in previous figures the masses and initial semi–major axis are unequal.

Table 2. The frequency of the various outcomes.

Run	Outcome frequency				
	Flyby	Exchange	Breakup	Triple	Unresolved
10d	2054	128	1256	429	133
11d	2290	127	1069	408	106
12d	2478	159	960	297	106
13d	1875	150	1255	514	206
20d	2534	98	871	371	126
21d	2702	107	832	288	71
22d	2821	101	820	181	77
10r	3485	21	196	250	48
11r	3344	21	298	294	43
12r	3437	16	398	138	11
20r	3434	14	221	260	71
21r	3522	13	202	236	27
22r	3561	11	301	116	11
30r	2867	50	673	308	112
31r	3051	56	587	233	73
32r	3184	50	564	140	62
40r	3143	36	507	242	74
41r	3268	34	448	208	42
42r	3328	36	454	142	40
50r	3669	6	51	225	49
51r	3679	2	156	162	1
52r	3674	3	305	16	2
60r	3755	0	31	186	28
61r	3754	1	116	127	2
62r	3761	2	220	17	0

to be bound and its orbital elements were solved for giving a new semi–major axis, a_3 and eccentricity, e_3. As the total energy was negative, at least one bound pair always exists. The other two particles were then considered. If their separation from the most tightly bound pair was less than $2a_3$ the stars were still considered to be strongly interacting and thus the encounter was unresolved. If the pair separation was larger, the orbital elements of the second pair were solved for, neglecting any interaction with the first pair. If the resulting eccentricity, e_4, was less than 1, we concluded two bound binaries existed and we solved for the second semi–major axis, a_4.

If the separation of the two new binaries was increasing, and the kinetic energy of the centres–of–masses of the binaries exceeded the binary–binary binding energy, we assumed the binaries would recede to infinity and we had a flyby or exchange, depending on the membership of the respective binaries. Else we considered the encounter unresolved. Note that this is an approximate condition, unlike the analogous case for three body scattering; in practise the separations are sufficiently large to ensure that few if any of these cases were misclassified as resolved.

If the second pair of particles was not bound to each other, we considered the particle furthest from the most tightly bound pair. If this particle was receding from the remaining binary, and its kinetic energy exceeded its binding energy relative to the other three particles, it was considered

to be escaping; if not, the encounter was still in resonant interplay and was unresolved. Given that the furthest particle was escaping, we now considered the remaining particle. We solved for the orbital elements of the third particle about the new binary, treating the binary as a point mass at its centre–of–mass. If the resulting eccentricity, $e_t > 1$ the third star was unbound and we concluded that we had a binary and two single stars. If $e_t < 1$ the third star was bound to the binary and we solved for its semi–major axis relative to the binary centre–of–mass, a_t. To determine whether the resulting triple was stable, we used the simple criterion, $3 \times a_3(1+e_3) < a_t(1-e_t)$ (Harrington 1975, but see Kiselva *et al.* 1994).If this criterion was satisfied, we assumed the triple was stable for timescales much larger than the orbital timescales, while if it failed we assumed the triple was unstable. Unstable triples are expected to decay to a binary and a single star, with the new binary semi–major axis drawn from a distribution approximately equal to that for resonant binary–single scattering at the same total energy and angular momentum. The approximate nature of the triple stability criterion is not a concern at this level of approximation; relatively few cases are close to being marginally stable and if the onset of instability is slow then for triples in globular clusters, encounters from field stars are likely to determine the future dynamical evolution of the system. A similar argument holds for binaries where the energy transfer was to the binaries and the analysis suggests the stars will not escape to infinity. For bound binary trajectories with apocentres $\gg a_{3,4}$, orbital periods become long and in real clusters field star perturbations on the quadruple start to become significant, the system is no longer dynamically isolated and for us to continue the integration further becomes irrelevant physically.

3 DYNAMICS AND CROSS–SECTIONS

For comparison with binary–single calculations and in order to calculate physical interaction rates, it is useful to calculate (normalised) cross–sections for a process to take place during an encounter. This is particularly important for comparing runs done with different $a_{1,2}, M_i$ and with different b_{max}.

We define the cross–section for a process, X, to be $\sigma_X = f(X)\pi b_{max}^2$, where $f(X)$ is the fraction of the total encounters in that run where X occurred (Hut & Bahcall 1983, Sigurdsson & Phinney 1993). We define a normalised cross–section, $\tilde{\sigma}_X$ by

$$\tilde{\sigma}_X = \frac{\sigma_X}{\pi(a_1^2 + a_2^2)} \left(\frac{v_\infty}{v_c}\right)^2. \quad (4)$$

This can be compared with the similar definition for binary–single scattering (Sigurdsson & Phinney 1993). The normalisation to the binaries geometric cross–section reduces to the binary–single case as $a_2 \to 0$ while the velocity ratio corrects for gravitational focusing. However, because of the different scaling with a_i for p, the resulting rates are not as simple as for the binary–single case.

A quantity of particular interest is the rate at which a given process X occurs in a cluster (core) of density $n\,\mathrm{pc}^{-3}$ and velocity dispersion v_s. If there are binaries (of the appropriate semi–major axis) in the cluster (core), constituting some fraction f_b of the total number of stars, then we expect binaries to encounter each other at some characteristic rate, R_X, with corresponding mean time between X occurring, $T_X = R_X^{-1}$. For a cluster with 1–D line–of–sight dispersion v_s', we expect the mean binary encounter velocity $v_\infty \sim v_s \sim \sqrt{3}v_s'$, as the binaries encounter each other with the full 3–D relative velocity drawn from the underlying velocity distribution, correcting for equipartition. Deprojection of the low dispersion foreground and background contamination, and the weighing of gravitational focusing provides additional corrections of order 10% (see Sigurdsson & Phinney [1995] for discussion).

The rate for a process to take place for a given binary moving in the cluster (core) is simply

$$R_X = \langle f_b n \sigma_X v \rangle. \quad (5)$$

It is important in using this approximation to distinguish the *global* binary fraction, that is the fraction of all stars that are binaries, from the local binary fraction with the relevant range of masses and semi–major axis. Relaxation in a cluster may lead to a the fraction of binaries with massive primaries in the core being higher than the global binary fraction; while dynamical evolution will decrease the core binary fraction (see Sigurdsson & Phinney 1995, Hut *et al.* 1992). A useful first approximation is to assume a global binary fraction of 0.5, with a uniform distribution in semi–major axis. Then per decade in semi–major axis, 10% of the stars are binaries with a semi–major axis in that range. Solving for T_X substituting $\tilde{\sigma}_X$ and eliminating v_c^2 we find

$$T_X = \left\langle \frac{\langle 1/v_\infty \rangle^{-1}}{\pi f_b n (a_1^2 + a_2^2) g(M) \left(\frac{M_1 M_2}{a_1} + \frac{M_3 M_4}{a_2}\right)} \frac{1}{\tilde{\sigma}_X} \right\rangle, \quad (6)$$

where $g(M) = GM_T/(M_1 + M_2)(M_3 + M_4)$. It is useful to scale T_X to the cluster parameters of interest. Writing $n = 10^4 n_4\,\mathrm{pc}^{-3}$, $v_\infty = 10 v_{10}\,\mathrm{km\,s}^{-1}$ and defining $a_{1,2} = a_{1,2}/AU$ and $M_i = M_i/\mathrm{M}_\odot$, we can write

$$T_X = \frac{1.5 \times 10^{10}}{f_b g(M) n_4} \left((a_1^2 + a_2^2)(E_{12} + E_{34})\right)^{-1} \left\langle \frac{1}{v_\infty} \right\rangle^{-1} \frac{1}{\tilde{\sigma}_X}\ \mathrm{y}, \quad (7)$$

where we have defined $E_{12} = M_1 M_2/a_1$ and $E_{34} = M_3 M_4/a_2$ with the masses in solar masses and the semi–major axis in AU as before.

Table 3 shows the normalised cross–section for exchanges, breakups and formation of stable triples for the different runs.

An interesting result is the relatively low cross–section for exchange, with a significantly higher cross–section for formation of stable triples at all semi–major axis ratios considered. As expected the relative cross–section for breakup of one of the binaries is large and increases both with v_∞/v_c and a_2/a_1. The fraction of unresolved encounters is small, except for the hardest set of runs with $a_1 = a_2$. We don't expect the unresolved encounters to contribute disproportionately to the close approaches; they mostly consist of resonances with one or two stars well separated from the other stars, but with insufficient energy to reach infinity; the other unresolved encounters consist of unstable triples. We expect any "memory" of the initial conditions to have been forgotten during the resonances, and the resonances are resolved with a distribution exactly similar to the resonances already resolved in that run, providing a few % correction

Table 3. Cross-sections for outcomes.

Run	$\tilde{\sigma}$(outcome)		
	Exchange	Breakup	Triple
10d	0.12	1.2	0.40
11d	0.23	2.0	0.75
12d	0.59	3.5	1.1
13d	0.069	0.58	0.24
20d	0.14	1.2	0.51
21d	0.30	2.3	0.80
22d	0.56	4.5	1.0
10r	0.014	0.14	0.17
11r	0.029	0.41	0.41
12r	0.044	1.10	0.38
20r	0.012	0.23	0.27
21r	0.027	0.42	0.49
22r	0.046	1.25	0.24
30r	0.049	0.66	0.30
31r	0.11	1.2	0.46
32r	0.20	2.2	0.55
40r	0.053	0.75	0.36
41r	0.10	1.3	0.61
42r	0.21	2.7	0.83
50r	0.0013	0.011	0.049
51r	0.00086	0.067	0.070
52r	0.0026	0.26	0.014
60r	0	0.010	0.060
61r	0.00065	0.075	0.082
62r	0.0026	0.28	0.022

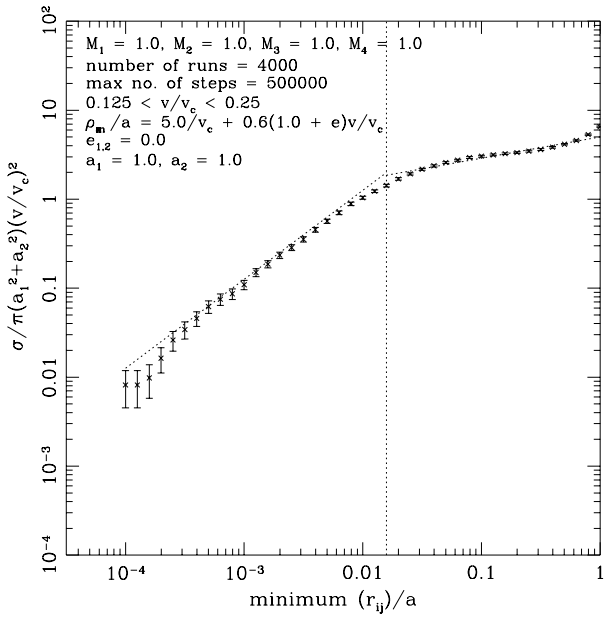

Figure 4. The cumulative cross–section for pairwise close approach, $r_{ij}, i = 1-4, j = i-4$, for particles i, j. The plot shown is for equal mass binaries with equal semi–major axis. The separation is scaled to the geometric mean of the semi–major axis, $a = (a_1 a_2)^{1/2}$, and the cross–section normalised to the geometric cross–section of the binaries and corrected for gravitational focusing. The solid lines show the piecewise power law fit to the cross–section, with the dotted line showing the formal breaking point between the two fits, r_b. The error bars are the standard error due to finite sampling per separation bin.

to the cumulative cross–sections for close approach at small r_{min} and adding to the cross–sections for different outcomes in the same proportion as the resolved encounters (Heggie 1988, Sigurdsson & Phinney 1993). Note that for the high a_1/a_2 runs we find a significant fraction of breakups of the wider binary despite the larger b_{max} at constant C. With a_1 this large, these distant encounters can still significantly perturb the wider binary.

3.1 Close Approach

A primary goal of this work is to estimate the rate of tidal interactions during binary–binary encounters in globular clusters, specifically encounters by hard binaries in the cluster cores. In order to do that, it is desirable to calculate the cumulative (normalised) cross–section for close approach between any pair of stars during an encounter, averaged over all of the binary phase space. Examples of these cross–sections are shown in Figures 4–8, for different mass ratios, semi–major axes and velocities. It is useful to fit the (normalised) cross–sections with a simple broken power–law, as shown in Figure 4 (see Hut & Bahcall 1983, Sigurdsson & Phinney 1993 for comparable fits for binary–single scattering).

To produce a power law fit, we assume the cumulative cross–section,

$$\tilde{\sigma}(\min\{r_{ij}\} \le r_{min}) = \sigma_0 \left(\frac{r_{min}}{a}\right)^{\gamma}. \quad (8)$$

In the case of binary–single scattering there is only one length scale, a, to normalise the "closeness" of approach. Here we have two length scales, a_1, a_2, and the normalisation is more ambiguous. We find it useful to scale to the geometric mean $a = \sqrt{a_1 a_2}$ and this is what is plotted in Figures 4–8 and is the normalisation used for calculating rates later. The choice of a is somewhat arbitrary for $a_1 \neq a_2$ and comparisons of cross–section calculated by different authors must be done with care.

To fit for σ_0, γ, we applied a piecewise (unweighted) least squares fit to the log of the cumulative cross–section vs. $\log r_{ij}$. The resulting fits are shown in Table 4. We define an additional parameter r_b, the separation at which we switch from one power law to the other. For $\min r_{ij} \le r_b$, $\sigma_0 = \tilde{\sigma}_1$ and $\gamma = \gamma_1$, whereas for $\min r_{ij} > r_b$ $\tilde{\sigma}_2, \gamma_2$ should be used respectively. r_b is plotted as a dotted line in Figure 4 for illustrative purposes. Formally r_b is defined to be where the fits cross; in practice this is close to the "knee" of the cumulative cross–section curve as desired. Because we oversample to large impact parameters, we discard the outermost point ($r_{ij} = a_2$) in the cumulative cross–section when producing the fit. It is necessary to use large enough impact parameters to be certain the cross–section for close approaches has converged, but for our purposes we are not interested in the weak perturbations to the semi–major axis caused by the widest flybys. For the high velocity runs with

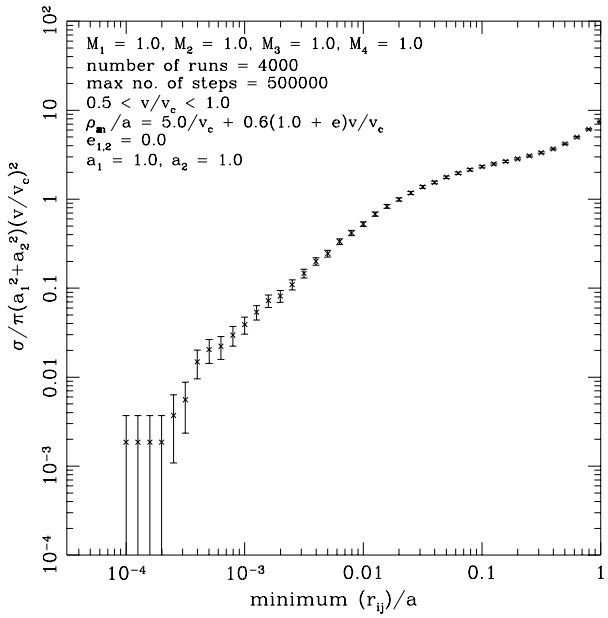

Figure 5. The cumulative cross–section for close approach for the high velocity run for equal mass and semi–major axis binaries.

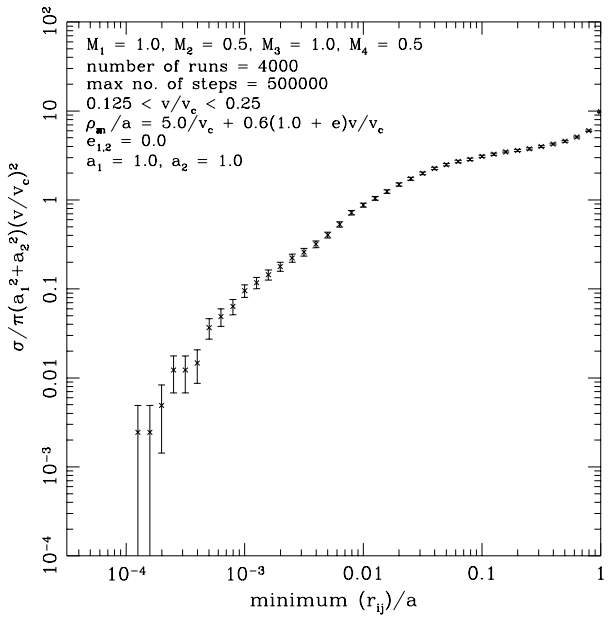

Figure 6. The cumulative cross–section for close approach for unequal mass and equal semi–major axis binaries.

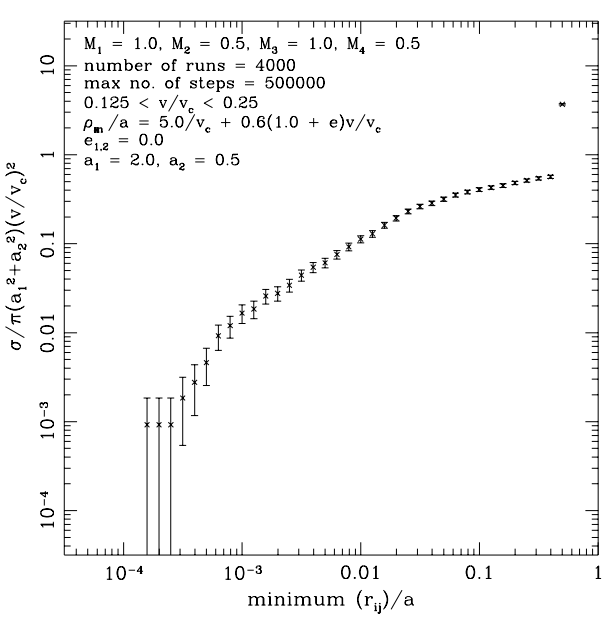

Figure 7. The cumulative cross–section for close approach for unequal mass and unequal semi–major axis binaries. There is a sharp turnup in cross–section for $r_{ij} = a_2$, this occurs because of the large number of encounters producing weak perturbations to the tighter binary. The discrete binning in r_{ij} does not resolve the turnup in cross–section.

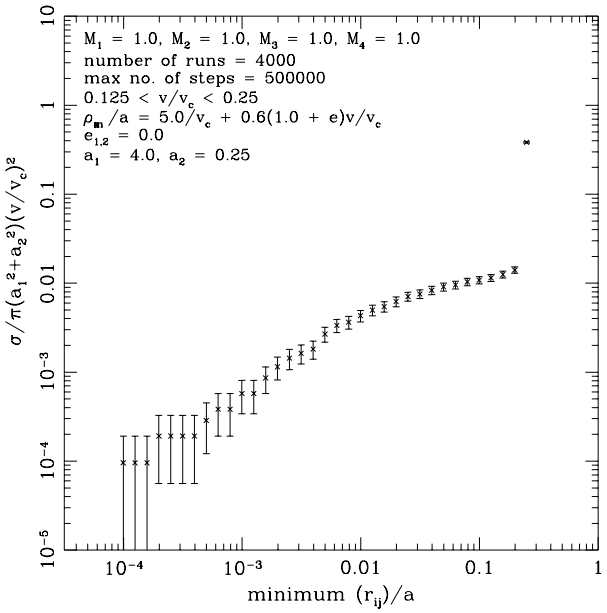

Figure 8. The cumulative cross–section for close approach for equal mass and unequal semi–major axis binaries.

Table 4. The power law fits for $\tilde{\sigma}(r_{\rm min})$.

Run	$\tilde{\sigma}_1$	$\tilde{\sigma}_2$	γ_1	γ_2	$r_{\rm b}$
10d	130	5.0	1.0	0.24	1.6×10^{-2}
11d	160	4.8	1.1	0.27	1.8×10^{-2}
12d	210	5.7	1.3	0.41	1.7×10^{-2}
13d	160	5.2	1.1	0.24	1.6×10^{-2}
20d	150	6.0	1.1	0.32	1.8×10^{-2}
21d	230	6.4	1.3	0.39	2.0×10^{-2}
22d	120	6.8	1.2	0.46	2.0×10^{-2}
10r	28	0.61	1.2	0.42	7.4×10^{-3}
11r	9.5	0.73	0.98	0.39	1.3×10^{-2}
12r	21	0.49	1.3	0.41	1.5×10^{-2}
20r	5.8	0.9	0.86	0.35	2.6×10^{-2}
21r	4.6	0.86	0.86	0.46	1.5×10^{-2}
22r	4.0	0.61	0.98	0.49	2.2×10^{-2}
30r	80	2.2	1.1	0.26	1.4×10^{-2}
31r	40	2.1	1.0	0.31	1.4×10^{-2}
32r	20	2.2	1.0	0.47	1.6×10^{-2}
40r	49	2.7	1.1	0.35	2.1×10^{-2}
41r	34	2.6	1.0	0.37	1.7×10^{-2}
42r	96	2.8	1.3	0.49	1.3×10^{-2}
50r	0.27	0.031	0.9	0.43	1.0×10^{-2}
51r	15	0.019	1.8	0.42	8.0×10^{-3}
52r	0.038	-	0.95	-	-
60r	0.41	0.027	1.1	0.43	1.7×10^{-2}
61r	0.11	0.027	0.94	0.55	2.7×10^{-2}
62r	0.048	-	0.89	-	-

$a_1 = 16a_2$ a single power law fit was adequate for all r_{ij} as indicated in the table.

The error–bars shown in Figures 4–8 show the standard deviation due to sampling noise from the finite number of encounters per bin. As the cross–section is cumulative the errors are systematically smaller at larger r_{ij}, hence it is not appropriate to weight the least squares fit by the errors.

As all the runs presented here are for $e_{1,2} = 0$ there might be some concern that for binaries with a thermal eccentricity distribution, as might be expected in globular clusters, the cross–section for close approach could be substantially larger than inferred from these simulations. To explore this we performed some runs with $e_{1,2}$ drawn from a thermal probability distribution, $P(e_i) = 2e_i$, and compared the ratio of cumulative cross–section for close approach for the eccentric and zero eccentricity binaries.

The result is shown in Figure 9. As can be seen from the figure, the ratio is approximately $1.7 = 1 + < e >$, over a large range in r_{ij}/a. The ratio rises at small r_{ij}/a, and results from other runs with $a_1 \neq a_2$ and $e_{1,2}$ thermal suggest this is significant. The ratio approaches unity at $r_{ij}/a = 1$ by definition. We conclude that allowing for an eccentricity distribution increases the cross–section for collisions by a factor of ~ 1.7, except for $r_{ij}/a \sim 10^{-4}$ for which the correction is somewhat larger. The same effect is seen for $a_2 \neq a_1$ but somewhat more pronounced. A possible concern is that this not a real dynamical effect, but simply the high eccentricity end of $a_2(1 - e_2)$ periastron passage. To check that this was not the case we made two checks: we truncated the eccentricity distribution at $e_{1,2} = 0.98$ and checked the increase in relative cross–section was still present, as it was, and we compared the initial periastron separation for each binary with $\min r_{ij}/a$. The closest approaches were predominantly due to binaries with $e_{1,2} \sim 0.5$, not encounters with very high initial binary eccentricity.

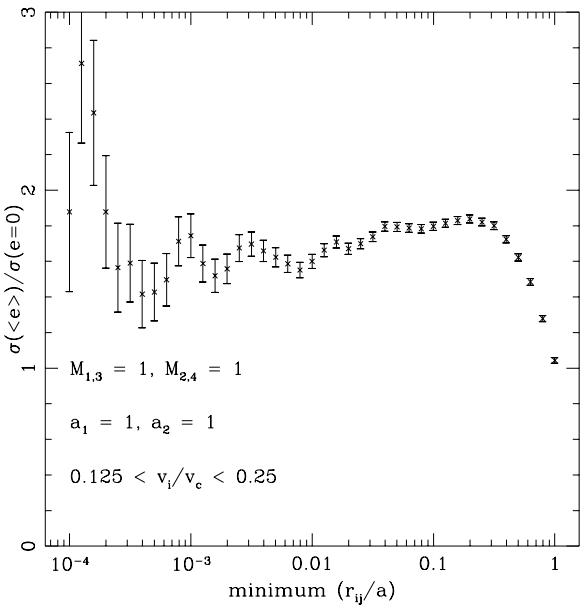

Figure 9. The ratio of cumulative cross–section for close approach for the for equal mass, equal semi–major axis binaries for zero eccentricity and for $P(e) = 2e$ runs. The errorbars show the standard error due to finite sampling.

3.2 Hardening of Binaries by Fly-by Encounters

We now consider the effects on the binaries of fly-by encounters. Such events are common compared to other processes such as exchanges, or the formation of triples as shown in Table 2. In Figures 10 and 12, we plot the distribution of semi-major axes a_1', and a_2' of the two binaries after a fly-by encounter for $a_1 = a_2$ and $a_1 = 4a_2$ respectively. As expected the distribution is symmetric for the equal semi–major axis binaries. The empty region in the upper right hand corner is forced by energy conservation, while angular momentum conservation prevents both binaries from hardening a lot simultaneously. For $a_1 = 4a_2$ most of the encounters produce a very weak perturbation in a_2 compared with a_1, as expected.

Figures 11 and 13 show the differential cross–sections for change in semi–major axis (cf. Davies *et al.* 1994, Sigurdsson & Phinney 1993, Hut & Bahcall 1983). For binary–single scattering, we expect $d\sigma/d\Delta \propto (1+\Delta)^{-4.5}$ for strong encounters (Heggie 1975), where $\Delta = \delta E_b/E_b$ is the fractional change in binary binding energy. In semi–major axis space we expect $d\sigma/da_i \propto a_i^{2.5}$ for strong encounters. The dotted line in Figures 11 and 13 shows a $a_i^{2.5}$ power law, the differential cross–section shows an approximate fit to

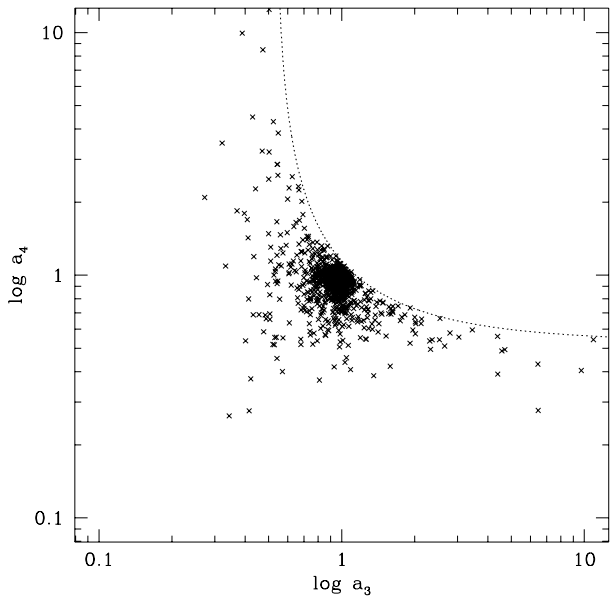

Figure 10. Plot of $\log a_3$ against $\log a_4$, for flybys for equal mass and initial semi–major axis binaries. There is a "forbidden" region excluded by energy conservation, bounded by the dotted line in the figure. The distribution in a_3, a_4 is roughly symmetric as expected. The changes in semi–major axis included 775 encounters where $a_3 < a_1$ and $a_2 < a_4$, 139 encounters where both binaries increased semi–major axis, and 549 and 591 encounters where one binary increased its semi–major axis and the other decreased, respectively.

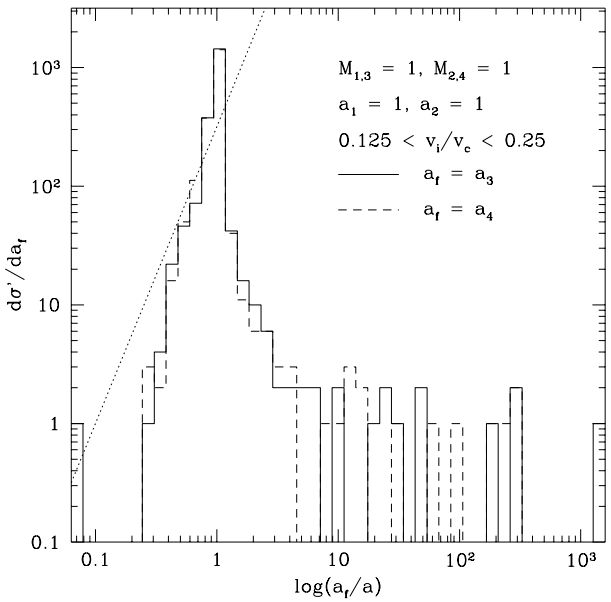

Figure 11. Distribution of final semi–major axis. The solid histogram show the distribution for a_3, the dashed line shows the distribution for a_4. The cross-section is unnormalised. The dashed line shows the distribution in a_i expected from Heggie's law for binary–single scattering, $d\sigma/da_i \propto a_i^{2.5}$. The distribution shown in the figure is for equal mass binaries and $a_1 = a_2$. As expected, the distributions in a_3, a_4 are equal to within poisson noise. The spike in the distribution at $a_{3,4} = 1$ is due to the large number of wide encounters producing small changes in semi–major axis.

Heggie's law over an interesting range in $\delta a/a$ for a sufficiently large δa. For weak perturbations, the differential cross–section diverges with b_{max} whereas for very strong encounters the falloff in cross–section is somewhat steeper than expected from Heggie's law. It is interesting to note that resonant flybys do not lead to large changes in binding energy compared to binary–single encounters. For other classes of outcome we defer discussion of the changes in energy to a later paper.

3.3 Application of Cross–Sections to Compute Rates in Globular Clusters

We now apply the cross–sections computed above to models of globular clusters. The calculated rates are listed with the cluster parameters in Table 5. Substituting equation 8 into equation 7, and approximating $\langle 1/v_\infty \rangle^{-1} = v_s$ we get the rate of collisions

$$T_c = \frac{1.5 \times 10^{10}}{f_b g(M) n_4 v_s} \left((a_1^2 + a_2^2)(E_{12} + E_{34}) \right)^{-1} \frac{(a_1 a_2)^{\gamma/2}}{\tilde{\sigma}_0 (r_{min})^\gamma} \, \mathrm{y}, \quad (9)$$

where $\gamma = \gamma_1, \tilde{\sigma}_0 = \tilde{\sigma}_1$ for $r_{min} \leq r_b$, and $\gamma = \gamma_2, \tilde{\sigma}_0 = \tilde{\sigma}_2$ for $r_{min} > r_b$. Table 5 shows a representative set of T_C for a range of cluster parameters, and for binaries containing two $0.7\mathrm{M}_\odot$ main–sequence stars and for binaries containing a $1.4\mathrm{M}_\odot$ compact star and a $0.7\mathrm{M}_\odot$ main–sequence star respectively. The binary separation assumed is shown for a_1 in AU, with a_1/a_2 then as given in column 5. For the calculation we choose $r_{min} = f_t R_*$, where R_* is the stellar radius,

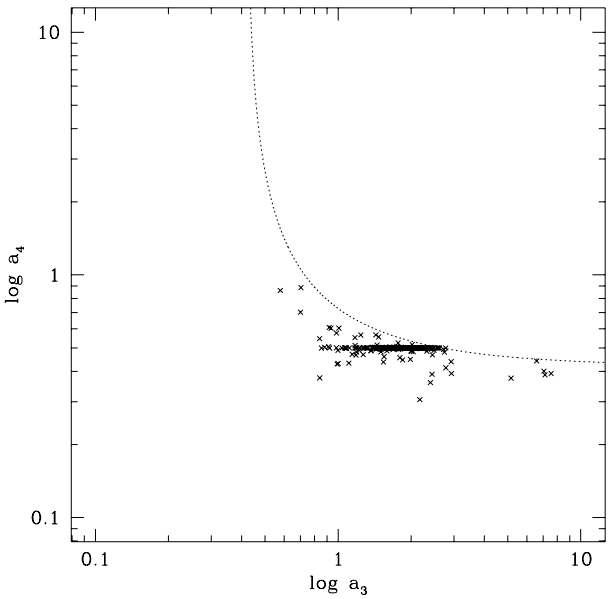

Figure 12. Plot of a_3 against a_4, for flybys for equal mass and unequal initial semi–major axis binaries. The dotted line shows the "forbidden" region excluded by energy conservation. The changes in semi–major axis included 973 encounters where $a_3 < a_1$ and $a_2 < a_4$, 770 encounters where both binaries increased semi–major axis, 648 encounters where $a_3 > a_1$ and $a_4 < a_2$, and 1094 encounters where $a_3 < a_1$ and $a_4 > a_3$.

Table 5. The timescale for tidal interaction or stellar collision, T_C (in years), for a binary with semi–major axis a_1 encountering a binary with semi–major axis a_2 in various globular cluster models, assuming $f_b = 1$ in the core for the semi–major axis used. a_1 is shown in AU, and $M_\star$ is the mass of the more massive star in each binary in solar masses. v_s is given in km s^{-1}.

$n_\star$	v_s	a_1	$\frac{v_\infty}{v_c}$	$M_\star$	a_1/a_2	T_c
10^2	3	100	0.85	0.7	1	1.2×10^{12}
			0.70		2	6.0×10^{11}
			0.54		4	8.1×10^{10}
			0.29		16	5.3×10^{11}
10^2		100	0.74	1.4	1	6.0×10^{11}
			0.60		2	1.3×10^{12}
			0.46		4	3.0×10^{11}
			0.25		16	7.7×10^{11}
10^2	10	10	0.90	0.7	1	2.0×10^{12}
			0.73		2	2.0×10^{12}
			0.57		4	1.0×10^{12}
			0.31		16	6.7×10^{12}
10^2		10	0.78	1.4	1	1.3×10^{12}
			0.63		2	2.2×10^{12}
			0.49		4	8.1×10^{11}
			0.27		16	7.2×10^{12}
10^4	5	10	0.45	0.7	1	3.3×10^{9}
			0.37		2	5.0×10^{9}
			0.28		4	3.1×10^{9}
			0.15		16	2.2×10^{10}
10^4		10	0.39	1.4	1	6.8×10^{9}
			0.32		2	4.4×10^{9}
			0.25		4	1.5×10^{9}
			0.13		16	1.9×10^{10}
10^4	10	1	0.28	0.7	1	5.2×10^{9}
			0.23		2	7.8×10^{9}
			0.18		4	3.4×10^{10}
			0.10		16	8.3×10^{10}
10^4		1	0.25	1.4	1	4.2×10^{9}
			0.20		2	9.3×10^{9}
			0.16		4	1.5×10^{10}
			0.084		16	7.6×10^{10}
10^6	10	0.3	0.16	0.7	1	8.0×10^{7}
			0.13		2	1.9×10^{8}
			0.10		4	1.2×10^{8}
			0.053		16	9.4×10^{8}
10^6		0.3	0.16	1.4	1	6.0×10^{7}
			0.11		2	1.5×10^{8}
			0.085		4	1.8×10^{8}
			0.046		16	6.9×10^{8}
10^6	15	0.1	0.13	0.7	1	2.8×10^{8}
			0.11		2	6.5×10^{8}
			0.085		4	1.5×10^{8}
			–			
10^6		0.1	0.10	1.4	1	2.1×10^{8}
			0.095		2	4.7×10^{8}
			0.074		4	3.1×10^{8}
			0.04		16	9.3×10^{8}

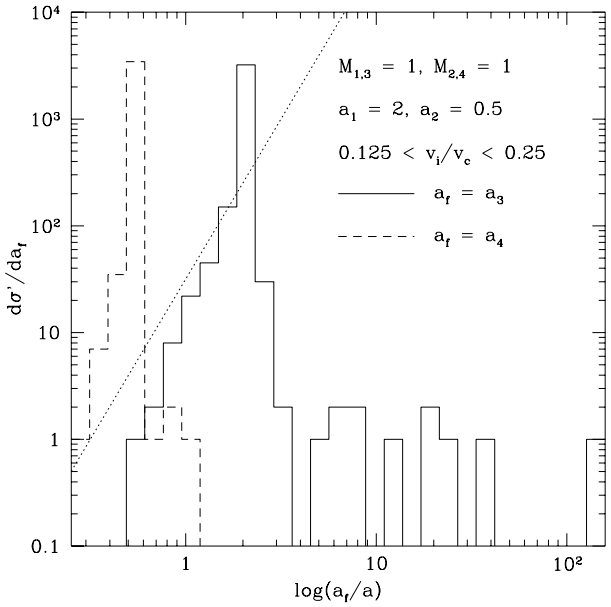

Figure 13. Distribution of final semi–major axis. The solid histogram show the distribution for a_3, the dashed line shows the distribution for a_4. The cross-section is unormalised. The dashed line shows the distribution in a_i expected from Heggie's law for binary–single scattering, $d\sigma/da_i \propto a_i^{2.5}$. The distribution shown here is for equal mass binaries and $a_1 = 4a_2$, as expected the distributions in a_3, a_4 are different, a_4 showing a much narrower spread from its initial value. Rather surprisingly, Heggie's law still fits well for strong perturbations to the tighter binary, for $a_4 \sim 1/2a_2$. The spike in the distribution at $a_3 = 2, a_4 = 0.5$ is due to the large number of wide encounters producing small changes in semi–major axis.

and $f_t \sim 3$ for main–sequence stars, with $f_t R_*$ being the separation at which tidal effects become significant in these encounters (Press & Teukolsky 1977). As before, the masses are in solar masses and radii in AU. The timescales in Table 5 are calculated assuming $f_b = 1$, that is all the stars in the cluster (core) are binaries with the appropriate mass and semi–major axis. In practise $f_b < 1$, possibly much less, and the total collision rate represents an average over all binary masses and semi–major axes.

A typical globular cluster core will contain about $N_* \sim 10^4$ stars. Here we follow observational conventions and count a binary as a single "star" when figuring N_*. Approximating the total collision rate as coming from a constant density core and neglecting contributions due to binary interactions outside the core, an approximation for the total number of collision products observed in a cluster is given by

$$N_c = f_e f_d f_b^2 N_* \frac{\tau}{T_c}, \tag{10}$$

where τ is the characteristic lifetime over which the collision product (eg. a blue straggler) is observable. Here we separate the fractional binary density in the core, f_d and the binary fraction in the appropriate semi–major axis range, f_b. We also allow for a factor f_e to correct for the eccentricity distribution. For most cases $f_e \sim 1.7$, except noting that for $R_* \lesssim 10^{-3} a_2$ and $a_2 \ll a_1$, $f_e \sim 10$. The true

rate is the integrated rate over $T_c(M_i, a_i)$ given $f_b(M_i, a_i)$; however the uncertainty in the binary population distribution is very large and the systematic uncertainties in the integrand make a formal integral meaningless. An approximation to the true collision rate can be made by assuming that $O(6\%)$ of the stars are near the turnoff, and another $O(2-4\%)$ is in evolved remnants. Mass–segregation then increases the fractional density of these more massive stars in the core further. As a simple approximation we can also assume that the binary fraction, f_b, is about 0.1 per decade in semi–major axis independent of binary mass, and that the total initial binary population spans about 5 decades in semi–major axis, $a_i \sim 10^{-2} - 10^3\ AU$.

In an old globular cluster, the core binary population is dynamically modified by mass segregation and subsequent interactions. Hardening and breakup reduce the number of wide binaries but increase the fraction of binaries with semi–major axis, $\sim a_c$, such that $T_R(a_c) \sim \tau_r$, where τ_r is the cluster relaxation time and $T_R(a_c)$ is the characteristic time scale for a binary with semi–major axis a_c to change its semi–major axis by order $a_c/2$. The situation is further complicated by dynamical recoil during strong binary–single and binary–binary interactions, which tends to remove hardened binaries from the cluster core to the cluster halo where interaction timescales are long (see eg. Sigurdsson & Phinney 1995). Binaries ejected to the cluster halo then return to the cluster core on a relaxation timescale.

As can be seen from Table 5, the collision timescale for a binary of some semi–major axis a_1 interacting with a binary of semi–major axis $a_2 \leq a_1$ does not vary much from $a_1 = a_2$ to $a_1 \sim 10a_2$, but then becomes longer for $a_1 \gg 10a_2$. Thus we can use a meaningful average collision timescale for binaries with semi–major axis in the same decade span, and neglect collisional interaction for binaries with semi–major axis in different decade spans as being negligible by comparison. Consider three different clusters, with core densities, n, of $10^2, 10^4$ and $10^6\,\mathrm{pc}^{-3}$ respectively. Assuming typical concentration parameters of $W_0 = 6, 9, 12$ for multi–mass Michie–King models and a Salpeter initial mass–function, mass–segregation increases the fractional density of $0.7 + 0.7\mathrm{M}_\odot$ binaries of all semi–major axes from 0.06, to 0.08, 0.15 and 0.26 respectively, neglecting dynamical recoil. Typical τ_r are $10^{10}, 10^9$ and 10^8 years respectively, and we expect those main–sequence binaries dominating the interaction rate to have semi–major axes of $10 - 100AU$, $0.1 - 1AU$ and $< 0.1AU$ respectively. Assigning a binary fraction of $f_b(a_i = 10 - 100AU) \approx 0.2$ for the low density cluster, $f_d = 0.08$ and $f_e = 10$, we find the expected number of currently observable main–sequence collisions to be, $N_{BS}(n = 10^2\,\mathrm{pc}^{-3}) = 4(f_b/0.2)^2$ per 10^4 core stars for $\tau_{BS} = 5 \times 10^9$ years, and taking $T_c \approx 10^{11}$ years as indicated in Table 5. For the medium density cluster, we similarly find $N_{BS}(n = 10^4\,\mathrm{pc}^{-3}) = 40$ for $f_b(a_i = 0.1 - 1AU) = 0.2$, $f_d = 0.15$ and $f_e = 1.7$. A higher f_b may be appropriate as the interaction time scale is short enough for a substantial fraction of binaries to be hardened from larger semi–major axes to the optimum range for collisions. For the densest cluster, we expect f_d to be smaller than mass–segregation would indicate as dynamical recoil and breakup are likely to have been significant over the cluster history, so we take $f_e = 1.7$, $f_b(a_i \leq 0.1AU) = 0.1$ and $f_d = 0.1$, even though mass–segregation would suggest $f_d \sim 0.2 - 0.3$. Using these values we find $N_{BS}(n = 10^6\,\mathrm{pc}^{-3}) = 500$. However, the true number may be smaller still as exchanges and collisions may have reduced the fraction of core stars near the main–sequence turnoff relative to the evolved remnant stars (see Sigurdsson & Phinney 1995).

It is interesting to compare, for binaries in the same semi–major axis range, the timescales to breakup due to binary–binary interactions with the timescale to collision. Using the results in Table 3, and binary parameters as above, we find $T_{breakup}(n = 10^2\,\mathrm{pc}^{-3}) = 3 \times 10^{10}$ years, $T_{breakup}(n = 10^4\,\mathrm{pc}^{-3}) = 4 \times 10^{10}$ years and $T_{breakup}(n = 10^6\,\mathrm{pc}^{-3}) = 3 \times 10^9$ years. For the lowest density cluster, a binary is several times more likely to be broken up by a binary–binary interaction, than be involved in a stellar collision, whereas for the medium density cluster breakup and collision are about equally likely, and the chance of a breakup in a binary–binary collision in the densest cluster is somewhat less than the probability of a stellar collision.

3.4 Comparison with Previous Results

NGC 5053 is a very low density ($n = 8\,\mathrm{pc}^{-3}$), low dispersion globular, with 24 observed candidate bue stragglers (Nemec & Cohen 1989). Some controversy exists in the literature over whether the blue stragglers in this cluster must be due to merger through internal evolution of initially tight primordial binaries (Hills & Day 1976) or whether binary–binary collisions may have produced a significant fraction of the observed blue straggler stars (Leonard & Fahlman 1991).

We find that we cannot produce the 24 blue stragglers observed in NGC 5053 even with $f_b = 1$ for binaries with $a_1 \gtrsim 100AU$; rather we find, $T_c \approx 2 \times 10^{12}$ years, giving $N_{BS} = 2 - 3(f_e/10)(f_d/0.1)(f_b/0.2)^2$ for a total core population of 40,000 stars. The encounter rate is dominated by binaries with semi–major axes $\gtrsim 100\,AU$, and it is unlikely $f_b \gg 0.2$ for this semi–major axis range, as many binaries must be much tighter than this. It is very unlikely that mass segregation has increased the fraction of binaries with primaries of near turnoff mass to $\gg 0.1$ in this cluster; the relaxation time scale is very long and the concentration low ($c = 0.75$).

It is not necessary to produce all the blue stragglers through binary–binary collisions, as some undoubtedly formed through spiral–in of tight primordial binaries (see eg. Livio 1993). It is possible that the fraction of primordial binaries with initial semi–major axis small enough for them to merge in a globular cluster lifetime is a function of the globular cluster initial density and dispersion. It is also possible that the core density of low density globular clusters has decreased on timescales of few $\times 10^9$ years through tidal shocking by the galaxy, and that the collision rates were thus higher in the past. Note that for every blue straggler produced by collisions during binary–binary encounters in these globular clusters we expect $\gtrsim 10$ binaries to have been dynamically broken up, and thus the current binary fraction in the right semi–major axis range would be smaller now than in the past.

In the case of NGC 5053, we might require the core density to have been an order of magnitude higher within the lifetime of the currently existent blue stragglers, and a

large fraction ($\gtrsim 0.3$) of the core turnoff stars to have been in wide ($a \sim 100AU$) binaries. We do expect the binary fraction to have decreased with time, but we still expect the present core binary fraction to be ~ 0.25 if binary–binary collisions are to account for the blue stragglers. This would be apparent in high precision photometry of NGC 5053 as a prominent second main–sequence (Romani & Weinberg 1991). Alternatively low density clusters like NGC 5053 may form a significant number of wide triples, and collisions are frequent during triple encounters.

It is instructive to compare the collision rate due to binary–binary encounters with the collision rate due to binary–single encounters. For the sample clusters discussed above, we find binaries with those semi–major axes have collision timescales with a single main–sequence star of 4.6×10^{11}, 5.4×10^{9} and 1.8×10^{8} years respectively, and the expected number of blue stragglers formed is given by $N_{BS} = f_d f_b (1 - f_b) f_* N_* \tau / T_c$, where f_* is the fractional density of main–sequence stars at the turnoff in the core, corrected for mass segregation ($0.13, 0.2, 0.2$ respectively). Using the same f_b as above, we find the expected number of blue stragglers to be $0 - 1, 50$ and 1100 respectively. That is, in the low density clusters binary–single collisions rates are comparable to binary–binary collisions, and the binary–singles dominate in the denser clusters. As not that many blue stragglers are observed in globular clusters one might infer the binary fraction per decade in semi–major axis is less than the 0.1 used here and the global binary fraction somewhat less than 0.5, which is consistent with observational estimates (Pryor *et al.* 1989, Yan & Mateo 1994) while still allowing a sufficiently high collision rate to produce the blue stragglers and other stellar exotica observed.

4 CONCLUSIONS

Some care must be taken in considering the effectiveness of binary–binary collisions in globular clusters. The *global* binary fraction at zero age in clusters is probably $0.5 - 1.0$, comparable with that seen in the field. However, this includes binaries from near contact, $a_i \sim 0.01AU$, to extremely wide binaries, $a_i \gg 10^3 AU$. The former do not interact on short enough timescales to be of interest, except in core–collapsed clusters, and will in due course merge through their internal evolution; the latter are soft and have high encounter rates in all except the very lowest density clusters, and are broken up in a few dynamical timescales. The global binary fraction as a function of a_i seems to have an initial distribution of approximately 0.1 per decade in a_i, and that is the approximation we use above. However, the core population of binaries is modified by several processes, including mass–segregation, dynamical recoil, exchange and breakup. As a result the fraction of binaries in the core, per decade in a_i and at different masses varies with time and cluster parameters. In calculating the expected number of blue stragglers above we made some effort to correct for the dominant processes in the different clusters considered.

We find collision timescales for plausible binary populations comparable to the lifetime of the clusters, and an expected number of blue stragglers sufficient to account for a large fraction of the low density blue straggler population, but overestimating the population in the denser clusters. This can be understood in terms of the dynamical evolution of the globular cluster binary population, as breakup and ejection decreases the core population of binaries.

We have refrained here from discussing in detail the properties of the final state of the binaries. In particular, parameters of interest include the final distribution of semi–major axis, not just for the flybys and exchanges, but also the breakups and triples, and the resultant cross–sections for energy transfer and recoil velocity distribution. Also of interest are the eccentricity distributions of the various final binary states. Of particular interest to us are the properties of the system after it undergoes an inelastic collision. Simulations of such collisions have been performed using SPH (Davies *et al.* 1993, 1994, Goodman & Hernquist 1991, Sigurdsson & Hernquist 1993). Approximating the collision as a totally inelastic "sticky particle" merger, conserving momentum but not energy, allows a quick and reasonably accurate way of determining the properties of the merged systems, in particular whether they form a single merged star, or if the merged star is in a binary or even a triple, and if so what the orbital parameters and center of mass recoil velocity of the system containing the merged star is. An analysis of these properties is deferred to a second paper (in preparation).

It is clear that binary–binary interactions are significant for producing stellar exotica through collisions in globular cluster cores. Compared to binary–single interactions, the rates inferred suggest a modest global binary fraction in the cores of the denser clusters, in accord with previous estimates, with $f_b(\text{all } a_i) \sim 0.2$ and $f_b(a_i) \sim 0.05$ per decade in a_i, while in the low density clusters the blue straggler population is consistent with a somewhat higher binary population, with perhaps $> 10\%$ of the turnoff mass main–sequence stars in the core being in binaries with $a_i \sim 100AU$. Binary–binary collisions most likely dominate binary–single collisions in many low density clusters as suggested by Leonard (1989) and may account for a significant fraction of the blue stragglers observed.

ACKNOWLEDGEMENTS

We thank Dr. Sverre Aarseth for providing some of his integration subroutines. Research supported in part by funding provided via the 1995 RGO/IoA/MRAO Summer Student Vacation Course under the auspices of the RGO and the IoA and Hampshire LEA. MBD gratefully acknowledges the support of the Royal Society through a URF. SS thanks the PPARC for support.

REFERENCES

Aarseth, S., 1984, in Dynamics of Star Clusters, IAU Symp. 113. D. Reidel: Dordrecht, p.251
Binney J. J., Tremaine S., 1987, in Galactic Dynamics. Princeton, p.235
Bolte, M., 1991, ApJ, 376, 514
Bolte, M., Hesser, J.E., Stetson. P.B., 1992, ApJL, 408, L89
Davies, M.B., Benz, W., Hills, J.G., 1993, ApJ, 411, 285
Davies, M.B., Benz, W., Hills, J.G., 1994, ApJ, 424, 870
Davies, M.B., Benz, W., 1995, MN, 276, 876
Davies, M.B., 1995, MN, 276, 887
Ferraro, F.R., Fusi Pecci, F., Cacciari, C., 1993, AJ, 106, 2324

Goodman, J., Hernquist, L., 1991, ApJ, 378, 637
Goodman, J., Hut, P., 1989, Nature, 339, 40
Harrington, R.S., 1975, AJ, 80, 1081
Heggie, D.C., 1975, MN, 173, 729
Heggie, D.C., 1988, in The Few Body Problem. Ed. M.J. Valtonen, Kluwer Dordrecht, 213
Hills J.G., 1975, AJ, 80, 809
Hills J.G., 1992, AJ, 103, 1995
Hills J.G., Day, C.A., 1976, ApJL, 17, 87
Hoffer J.B., 1983, AJ, 88, 1420
Hut, P., Bahcall, J. N., 1983, ApJ, 258, 319
Hut, P., et al., 1992, PASP, 104, 981
Hut, P., McMillan, S., Romani, R., 1992, ApJ, 389, 527
Hut, P., 1995, in Millisecond Pulsars: A Decade of Surprise. ASP Conf. 72, ed. A.S. Fruchter, M. Tavani, D.C. Backer ASP San Francisco, 46.
Kiselva, L.G., Eggleton, P.P., Orlov, V.V., 1994, MN, 270, 936
Leonard, P.J.T., 1989, AJ, 98. 217
Leonard, P.J.T., Fahlman, G.G., 1991, AJ, 102, 994
Leonard, P.J.T., Linnell, A.P., 1992, AJ, 103, 1928
Livio, M., 1993, in Blue Stragglers. ASP Conf. 53, ed. R.A. Saffer ASP San Francisco, 3.
Mateo, M., Harris, H.C., Nemec, J., Olszewksi, E.W., 1990, AJ, 100, 469
McMillan, S., Hut, P., Makino, J., 1990, ApJ, 362, 522
McMillan, S., Hut, P., Makino, J., 1991, ApJ, 372, 111
McMillan, S., Hut, P., 1994, ApJ, 427, 793
Mikkola, S., 1983, MN, 203, 1107
Mikkola, S., 1984, MN, 207, 115
Mikkola, S., 1984, MN, 208, 75
Nemec, J.M., Harris, H.C., 1987, ApJ, 316, 172
Nemec, J.M., Cohen, J.G., 1989, ApJ, 336, 780
Press, W.H., Teukolsky, S.A.0, 1977, ApJ, 213, 183
Pryor, C., Smith, G.H., McClure, R.D., 1989, AJ, 92, 1358
Rasio, F.A., McMillan, S., Hut, P., 1995, ApJL, 438, L33
Romani, R.W., Weinberg, M.D., 1991, ApJ, 372, 487
Sigurdsson, S., Hernquist, L., 1992, ApJL, 401, L93
Sigurdsson, S., Phinney, E.S., 1993, ApJ, 415, 631
Sigurdsson, S., Davies, M.B., Bolte, M., 1994, ApJL, 431, L15
Sigurdsson, S., Phinney, E.S., 1995, ApJS, 99, 609
Valtonen, M., Mikkola, S., 1991, ARAA, 29, 9
Yan, L., Mateo, M., 1994, AJ, 108, 1810